Effects of noise in a cortical neural model

Maria Marinaro and Silvia Scarpetta
Dipartimento di Fisica "E. R. Caianiello", Salerno University, Baronissi (SA) IT, INFM Sezione di Salerno (SA) IT, and IIASS Vietri sul mare (SA), Italy
(Received 8 August 2003; published 29 October 2004)

Recently Segev *et al.* [Phys. Rev. E **64**, 011920 (2001); Phys. Rev. Lett. **88**, 118102 (2002)] made long-term observations of spontaneous activity of in-vitro cortical networks, which differ from predictions of current models in many features. In this paper we generalize the excitatory-inhibitory cortical model introduced in a previous paper [Scarpetta *et al.*, Neural Comput. **14**, 2371 (2002)], including intrinsic white noise and analyzing effects of noise on the spontaneous activity of the nonlinear system, in order to account for the experimental results of Segev *et al.* Analytically we can distinguish different regimes of activity, depending on the model parameters. Using analytical results as a guide line, we perform simulations of the nonlinear stochastic model in two different regimes, B and C. The power spectrum density (PSD) of the activity and the interevent-interval distributions are computed, and compared with experimental results. In regime B the network shows stochastic resonance phenomena and noise induces aperiodic collective synchronous oscillations that mimics experimental observations at 0.5 mM Ca concentration. In regime *C* the model shows spontaneous synchronous periodic activity that mimics activity observed at 1 mM Ca concentration and the PSD shows two peaks at the first and second harmonics in agreement with experiments at 1 mM Ca. Moreover (due to intrinsic noise and nonlinear activation function effects) the PSD shows a broad band peak at low frequency. This feature, observed experimentally, does not find explanation in the previous models. Besides we identify parametric changes (namely, increase of noise or decreasing of excitatory connections) that reproduces the fading of periodicity found experimentally at long times, and we identify a way to discriminate between those two possible effects measuring experimentally the low frequency PSD.

DOI: 10.1103/PhysRevE.70.041909 PACS number(s): 87.18.Sn, 05.40.Ca, 05.45.Xt

I. INTRODUCTION AND MOTIVATIONS

Spontaneous (and stimulation-driven) synchronized oscillatory activity has been observed in many in-vitro and in-vivo experiments [1–3].

The understanding of spontaneous activity of in-vitro networks [4–7] is a preliminary requirement for the comprehension of the network behavior inside the animal brain, where the dynamics are more complex due to the presence of external stimuli and of interactions among different parts of the brain. In particular, the understanding of the specific mechanisms underlying the spontaneous spatiotemporal pattern of activity is important for the comprehension of brain activity, especially in relation with epilepsy [8], the central pattern generator systems, etc.

Recently Segev *et al.* [4,5] have done accurate long-term measurements of the spontaneous activity of in-vitro cortical cells neural networks placed on multielectrode arrays. The effect of external Ca concentration on the spontaneous activity has been studied. They observed, for a critical range of Ca concentration, periodic synchronized bursting activity, that fades away after $\sim$20 min. Periodic synchronized bursting is observed at 1 mM Ca concentration and not at higher (2 mM) and lower (0.5 mM) concentrations. Their observations differ from prediction of current neural network models in many features. They try to model the phenomena performing numerical simulations of an integrate-and-fire network model with random connections. Adding (1) dynamic threshold and (2) activity-dependent synaptic connections, they reproduce much of the observed network activity, but do not obtain a complete explanation of the experimental results. For example, their numerical simulations capture the transition between aperiodic synchronized bursting versus periodic synchronized bursting when Ca concentration (and so model connection strengths) was increased, but they do not reproduce the transition from periodic synchronized bursting versus aperiodic activity observed experimentally when Ca concentration was increased over the critical interval. Moreover the experimental data show that the energy distribution over low frequencies has a broad band with power law decay that indicates the existence of positive long-range time correlations in the sequences of bursts; this behavior cannot be accounted for by the Segev *et al.* model. The interevent-interval (IEI) distribution at 0.5 mM Ca shows a very long tail (tens of seconds), decaying much more slowly than in the integrate-and-firing (IF) model. Finally, experimental results show that, after 1 mM Ca concentration was obtained, the high peaks of the power spectrum density (PSD), at first and second harmonic, become lower and lower with time, and after $\sim$20 min the PSD is almost flat. These PSD features (in particular the behavior at low frequency and the changes that happen in a time scale of several minutes) have not been explained by the models of Segev *et al.* [4,5], and as far as we know, until now the explanation is lacking. Patterns of spontaneous activity in cortical cultured networks were observed by other researchers [3,7]. Canepari *et al.* [3] observed transitions from asynchronous firing dynamics to synchronous firing dynamics when Ca2+ concentration was increased from 0.1 to 1 mM.

Here we model a cultured cortical cells network using a excitatory-inhibitory (EI) Cowan-Wilson-like [9] model ana-

lytically tractable, which enables us to study the source of spontaneous activity dynamics analytically. We analyze the macroscopic observables that describe the dynamics of the system as a function of the network parameters, exploiting effects of noise and nonlinearity.

We show that some insights and a good agreement with experiments can be obtained including intrinsic white noise in the spiking-rate excitatory-inhibitory (EI) neural network model. The model is based on the noiseless cortical model introduced in a previous paper [10] by one of us, Li, Hertz, which is able to imprint and retrieve oscillatory patterns when driven by noiseless oscillatory input (using a generalized hebbian learning rule). Here the model is studied to put in evidence its spontaneous activity and specifically the effects of noise on the dynamics are analyzed. The spatiotemporal patterns of spontaneous activity in our model is a consequence of the dynamics of the interacting excitatory and inhibitory units, and depends critically from the presence of noise and from the synaptic strengths of the EI network.

The results we have found, although referred to the work of Segev *et al.* [4,5], are of more general interest, indeed they connect the behavior of in-vitro neural networks to the one of nonlinear subthreshold and overthreshold systems in presence of noise.

The effects of noise in neural models is the focus of a lot of recent literature [11–13], from the single FitzHugh-Nagumo system point of view [13] to the IF homogeneous networks [12] or the phase-model coupled oscillators [11].

In Sec. II the model is described, in Sec. III–V analytical and numerical results are reported, and in Sec. VI there are discussions and conclusions.

II. MODEL

Our starting point in modeling is the stochastic Cowan-Wilson-like EI equations [10,9,14] governing the state variables, modeling the membrane potentials, $\mathbf{u}=\{u_1,\ldots,u_N\}$ and $\mathbf{v}=\{v_1,\ldots,v_N\}$, respectively, for the excitatory and inhibitory units:

$$\dot{u}_i = -\alpha u_i - \sum_j H_{ij} g_v(v_j) + \sum_j J_{ij} g_u(u_j) + \overline{F_i}(t), \qquad (1)$$

$$\dot{v}_i = -\alpha v_i + \sum_j W_{ij} g_u(u_j) + F_i(t). \qquad (2)$$

The unit outputs $g_u(u_1),\ldots,g_u(u_N)$ and $g_v(v_1),\ldots,g_v(v_N)$ represent the probabilities of the cells firing (or instantaneous firing rates) where g_u and g_v are sigmoidal activation functions that model the neuronal input-output relations. α^{-1} is a time constant (about few milliseconds, for simplicity it is assumed equal for excitatory and inhibitory units) modeling the membrane time constant, J_{ij} is the synaptic connection strength from excitatory unit j to excitatory unit i, W_{ij} is the synaptic connection strength from excitatory unit j to inhibitory unit i and H_{ij} is the synaptic connection strength from inhibitory unit j to excitatory unit i. Since in cortical area pyramidal cells have long range connections to other pyramidal cells and to inhibitory interneurons, while inhibitory interneurons generally only project locally, we assume J_{ij} and W_{ij} to be long range connections, and H_{ij} to be local. All these parameters are non-negative; the inhibitory character of the second term on the right-hand side of Eq. (1) is indicated by the minus sign preceding it. $\overline{F_i}(t)$ and $F_i(t)$ model the intrinsic noise, respectively, on the excitatory and inhibitory units, not included in the definition of u,v. In a (cultured) interacting neurons system noise can be due to several reasons, like thermal fluctuation, ionic channel stochastic activities, and many others. We take the noise $\overline{F_i}(t), F_i(t)$ to be uncorrelated white noise, such that $\langle F_i(t)\rangle = \langle \overline{F_i}(t)\rangle = 0$ and $\langle F_i(t)\, F_j(t')\rangle = \Gamma \delta_{ij}\delta_{t-t'}$, $\langle \overline{F_i}(t)\, \overline{F_j}(t')\rangle = \overline{\Gamma}\delta_{ij}\delta_{t-t'}$. Each such unit u_i, v_i represents a local assembly of pyramidal cells or local interneurons sharing common, or at least highly correlated, input. (The number of neurons represented by the excitatory units may be in general different from the number represented by the inhibitory units.) For reasons explained in the following, we choose the connection matrices J, H, W symmetric, apart from small random fluctuations. This symmetry does not imply symmetry of the total connection matrix $\left(\begin{smallmatrix} J & -H \\ W & 0 \end{smallmatrix}\right)$, indeed it is highly asymmetric, as well as the connections between excitatory and inhibitory neurons are still asymmetric in this scenario.

Network connectivity

Since the connectivity formation of the cultured system we want to model has grown randomly and spontaneously, we can reasonably assume that the strength of each connection is a function only of the type of presynaptic and postsynaptic neurons (excitatory or inhibitory), and of the distance between them, plus eventually some random quenched fluctuations. Recent estimation of connectivity in in-vitro rat cortical networks has shown long range connections, with arborization of the neurons of 1.2 ± 0.5 mm^2 [7], such that each neuron was connected with about 600 nearby neurons.

We will analyze two types of connectivity structures:

- In the first case, each excitatory unit is connected to all the other units of the model, while inhibitory units only project locally. In particular, J and W are long-range matrices given by

$$J_{ij} = j_0(1 + \epsilon \eta_{ij}^{(J)})/N,$$

$$W_{ij} = W_0(1 + \epsilon \eta_{ij}^{(W)})/N, \qquad (3)$$

and the matrix H is local $H_{ij}=h_0\delta_{ij}(1+\epsilon\eta_i^{(H)})$, where $\epsilon \ll 1$ and $\eta_{ij}^{(J)}$, $\eta_{ij}^{(W)}$, and $\eta_i^{(H)}$ are random quenched values, uniformly distributed between -1 and 1. When $\epsilon=0$, the three connection matrices commute each other and share a complete set of eigenvectors. In particular the principal eigenvector $\xi_0=(1/\sqrt{N},\ldots,1/\sqrt{N})$ has eigenvalues j_0, W_0, and h_0, while the others $N-1$ eigenvectors have eigenvalues 0, 0, and h_0, respectively. When $\epsilon>0$, the vector $\xi_0 = (1/\sqrt{N},\ldots,1/\sqrt{N})$ will still be an eigenvector of the connection matrices, apart from corrections of order $O(\epsilon/\sqrt{N})$. In this paper we take $\epsilon=0$, in a following paper, we will investigate the effects of order ϵ and ϵ^2 (numerical simu-

lations with small $\epsilon \neq 0$ give results qualitatively similar to the ones with $\epsilon = 0$).

• In the second case, we consider structured short-range connectivity, inspired by recent measurements [15,7]. We put one excitatory and one inhibitory unit on each site of a square lattice with L rows and M columns, so that there will be $N = \mathrm{LM}$ excitatory units and N inhibitory units. Each inhibitory unit is connected only locally, to the excitatory unit that is on the same site. Numbering the unit in a typewriter way, from 0 to $N-1$, we connect the i-th excitatory unit to the excitatory and inhibitory units that are on the eight sites numbered $i-1 \bmod N$, $i+1 \bmod N$, $i-M \bmod N$, $i+M \bmod N$, $i-M+1 \bmod N$, $i+M-1 \bmod N$, $i+M+1 \bmod N$, $i-M-1 \bmod N$. Therefore, each elements of J_{ij} is

$$J_{ij} = \begin{cases} j_0/8 & \text{if } |i-j| \bmod N = 1 \\ j_0/8 & \text{if } |i-j| \bmod N = M \\ j_0/8 & \text{if } |i-j| \bmod N = M \pm 1 \\ 0 & \text{otherwise.} \end{cases} \tag{4}$$

Analogously $W_{ij} = w_0/8$ if $|i-j| \bmod N = 1$ or M or $M \pm 1$, and is zero otherwise. H_{ij} is h_0 if $i=j$ and is zero otherwise.

Notice that, apart from the units on the boundary, each unit is connected to its four nearest neighbors and to its four next-nearest neighbors. Furthermore the connection matrices J and W are Toplitz matrices so that eigenvectors are the Fourier basis

$$\xi_n(j) = \frac{1}{\sqrt{N}} e^{i 2\pi n j/N} \tag{5}$$

and eigenvalues, given the notation $J_{ij} = J(i-j) = J(x)$, can be easily calculated: $j_n = \Sigma_{x=0}^{N-1} J(x) \cos(2\pi/N n x)$, and analogously for W. The highest eigenvalue of J is j_0 (and w_0 for W), corresponding to the eigenvector with $n=0$. H is diagonal and has all eigenvalues equal to h_0. We investigate also the case of structured short-range connectivity with open boundary conditions. In such a case the eigenvectors and eigenvalues are not known analytically and have to be computed numerically.

In experiments of Segev *et al.* [4] three networks are analyzed with different geometries and size: a small 50-cells with a quasi-one-dimensional (1D) 2 mm $\times$ 50 μm geometry, medium 10^4-cells networks, with a rectangular 2 mm $\times$ 2 mm geometry, and a large 2×10^6-cells network with a circular 11-mm-radius geometry.

When $L = \mathrm{M}$ our lattice model describes the 2D square geometry, while when $M=1$ and $L = \mathrm{N}$ there are only two connections for each site (left and right next-neighbor sites) and the model describes the quasi-1D geometry used in the experiments.

In both cases (3) and (4), all the matrices J, W and H commute each other and share a common set of eigenvectors given by the Fourier basis in Eq. (5).

In the next section the model dynamics is analyzed in terms of the eigenvectors and eigenvalues of the connection matrices. The procedure is the same for both the structured short-range connectivity (4) and the long-range connectivity that we have considered, since in both cases we know analytically the eigenvectors and eigenvalues of the matrices. In the open boundary conditions case we compute the eigenvalues numerically.

III. MODEL DYNAMICS

Using vectorial notation, the dynamics of the model is described by the 2N components vector $\{\mathbf{u}, \mathbf{v}\}$. Let us call $\{\overline{\mathbf{u}}, \overline{\mathbf{v}}\}$ the fixed point determined by $\dot{\mathbf{u}} = 0$, $\dot{\mathbf{v}} = 0$ with $\overline{\mathbf{F}}(t) = 0$, $\mathbf{F}(t) = 0$.

Linearizing Eqs. (1) and (2) around the fixed point $\{\overline{\mathbf{u}}, \overline{\mathbf{v}}\}$, eliminating $\mathbf{v}$ from the equations, and assuming noise to be only on the $\mathbf{v}$ units ($\overline{\Gamma} = 0$), we get

$$\ddot{\mathbf{u}} + (2\alpha - \mathsf{J})\dot{\mathbf{u}} + [\alpha^2 - \alpha \mathsf{J} + \mathsf{HW}]\mathbf{u} = -\mathsf{H}\mathbf{F}(t), \tag{6}$$

where $\mathbf{u}$ is now measured from the fixed point value $\overline{\mathbf{u}}$, and nonlinearity enters only through the redefinition of the elements of J, H, and W: $J_{ij} g_u'(\overline{u_j}) \to J_{ij}$, $H_{ij} g_u'(\overline{v_j}) \to H_{ij}$ and $W_{ij} g_u'(\overline{u_j}) \to W_{ij}$. We use bold and sans serif notation (e.g., $\mathbf{u}, \mathsf{J}$) for vectors and matrices, respectively.

The fixed point $(\overline{\mathbf{u}}, \overline{\mathbf{v}})$ is stable if the homogeneous associate equation of Eq. (6) has only decaying solutions $\mathbf{u}$. In particular, when J, H, and W share the same set of eigenvectors $\boldsymbol{\xi}_n$, denoting with j_n, W_n, and h_n their eigenvalues, the eigensolutions are

$$\mathbf{u}_n = e^{\lambda_n t} \boldsymbol{\xi}_n, \tag{7}$$

where

$$\lambda_n = -\frac{2\alpha - j_n}{2} \pm \frac{\sqrt{j_n^2 - 4 h_n W_n}}{2} \tag{8}$$

and the stability condition is $\mathrm{Re}[\lambda_n] < 0$, i.e., the real parts $\mathrm{Re}[\lambda_n]$ of the eigenvalues λ_n of the homogeneous system must be negative. The state vector $\mathbf{u}$ is a linear combination of all the eigenmodes, given by $\mathbf{u} = \Sigma_n c_n e^{\lambda_n t} \boldsymbol{\xi}_n + \mathrm{c.c.}$ in the absence of noise $\Gamma = 0$, therefore if all the n modes have $\lambda_n = \mathrm{Re}[\lambda_n] < 0$, and $\mathrm{Im}[\lambda_n] = 0$, the activity $\mathbf{u}$ simply decays toward the fixed point, stationary state (regime A). In regime A the isolated system is "quiet" and, each unit just fires randomly, each one uncorrelated with the others. Regime A corresponds to $j_n < 2\alpha$ and $j_n^2 \simeq 4 h_n W_n$. Besides the regime A, other interesting dynamic regimes can be considered. In the following we analyze two cases named, respectively, regimes B and C. The regime B arises when

$$\mathrm{Re}[\lambda_n] < 0 \quad \forall\, n$$
$$\mathrm{Im}[\lambda_n] = 0 \quad \forall\, n \text{ but one (call it } n = 0).$$

It means that excitatory connections are such that $j_0 < 2\alpha$ and $j_0^2 < 4 h_0 W_0$. In this regime, in absence of noise the system (after a transient with damped oscillations) settles down to the stable fixed point. However as we will see later, spontaneous collective aperiodic oscillations are induced by noise. The activity in presence of noise is similar to the one observed in-vitro by Segev *et al.* at 0.5 mM Ca concentra-

tion. The regime C is present when it exists at least an eigenvalue, let call it λ_0, such that

$$\mathrm{Re}[\lambda_0] > 0$$
$$\mathrm{Im}[\lambda_0] \neq 0.$$

It means that $2\alpha < j_0 < \sqrt{4h_0W_0}$. Therefore regime C occurs only in a critical interval of excitatory connections strength, such that excitatory principal eigenvalue j_0 is greater then 2α but lower then $\sqrt{4h_0W_0}$. In this regime spontaneous oscillations grow in the linear approximation. As one expects, the saturating nonlinearity stabilizes the limit cycle. The nonlinear model shows synchronous periodic activity spontaneously, as we will see later, similar to the experimental results observed at 1 mM Ca concentration.

When j_0 is so large that $j_0 > 2\alpha$ and $j_0 > \sqrt{4h_0W_0}$ the linear analysis predicts a divergence without oscillations. In this case strong nonlinear effects have to be taken in consideration. It has been observed by numerical simulations (Sec. V) that the system shifts to a new stable fixed point, around which oscillations are induced by noise.

The extracellular Ca2+ is known to affect synapse probability of transmitter release [17,18] and the action potential firing threshold (see Ref. [16]). The parameter of interest J, H, and W are actually products of connection strengths and gradients of the nonlinear terms evaluated at the equilibrium position; calcium concentration may affect both terms. So the effects of extracellular Ca2+ concentration may be multiple. We model the increase of Ca concentration as an increase of the excitatory connection strengths. Modeling the increase of Ca concentration as an increase of excitatory connections J and W (or at least as an increase of the excitatory-to-excitatory connection strength J), then both the transitions observed experimentally from 0.5 to 1 mM and from 1 to 2 mM Ca concentration could be accounted by the model. Indeed while a small increase in Ca concentration (and therefore a small increase of j_0 with respect to α) induces a transition in the model from regime B to regime C, a larger increase in Ca concentration (and therefore a larger increase of j_0) make the model to go out of regime C.

IV. REGIME B DYNAMICS AND STOCHASTIC RESONANCE EFFECTS

Starting from Eq. (6) we first analyze the self-correlation function of excitatory unit i, $C_i(t-t') = \langle u_i(t)u_i(t')\rangle - \langle u_i(t)\rangle \times \langle u_i(t)\rangle$ and the average self-correlation function $C(t-t') = \frac{1}{N}\Sigma_i C_i(t-t')$ in the regime B in presence of noise of amplitude Γ. The PSD, i.e., the Fourier transform $\tilde{C}(\omega)$ of $C(t-t')$, is the sum of N contributions given by

$$\tilde{C}^n(\omega) \propto \frac{h_0^2 \Gamma \tau_n^4}{(1+\omega^2\tau_n^2)^2} \tag{9}$$

when the eigenvalues are real and negative $\lambda_n = -1/\tau_n$, and by

$$\tilde{C}^0(\omega) \propto \frac{h_0^2 \Gamma \tau_0^4}{4(1+\omega_0^2\tau_0^2)}\left[\frac{2+\omega/\omega_0}{1+\tau_0^2(\omega+\omega_0)^2} + \frac{2-\omega/\omega_0}{1+\tau_0^2(\omega-\omega_0)^2}\right] \tag{10}$$

for the eigenvalue $\lambda_0 = -1/\tau_0 + i\omega_0$, with $\tau_0 > 0$, $\omega_0 \neq 0$. The contribution expressed by Eq. (9) is peaked at $\omega = 0$, while the contribution given by Eq. (10) is peaked at ω close to ω_0 (when $\tau_0\omega_0 < 1$). In regime B the PSD has contributions also from Eq. (10). Therefore the linear analysis predicts that noise induces in the regime B a collective oscillatory behavior in the neurons activity. This collective oscillatory behavior corresponds to a broad peak in the power-spectrum of the neurons activity near the characteristic frequency ω_0.

We perform numerical simulations of the nonlinear network model with the long-range connectivity and with the short-range connectivity. The values of parameters have been chosen in such a way to satisfy the conditions for the regime B. Similar results have been obtained in the long-range connectivity case (Figs. 1 and 2) and in the short-range connectivity model (Fig. 3). Noise induces spontaneous oscillations that are synchronous because $\boldsymbol{\xi}_0$ has real positive elements. Figure 1 shows the synchronous time behavior of the state variables $u_i(t)$, and its power spectrum density, when noise is $\Gamma = 0.0004$ in the $N = 10$ long-range connections model [Eq. (3)], in regime B. The signal $u_i(t)$ looks aperiodic on long time scale, being decorrelated over long time scale by the noise. This spontaneous aperiodic synchronous activity mimics the spontaneous aperiodic synchronous activity observed under 0.5 mM Ca (and 2.0 mM Ca) concentration in Ref. [5]. We compute the interevent-interval (IEI) between two successive bursting events. A peak of all u_i with intensity above 0.7 is defined as a synchronized bursting event. From the sequence t_n, specifying the location of the nth event, we compute the IEI histogram shown in Fig. 2. Figure 3(b) shows the IEI histogram of a short-range connectivity model [Eq. (4)] with $N = 100$ in regime B with noise $\Gamma = 0.001$. Notably, both IEI are in a good agreement with the experimental one observed at 0.5 mM Ca (see Fig. 5 of Ref. [5]). Both experimentally and in the model, the IEI shows a peak (at about 10 s) with a very long tail (around 40–60 s the histogram is still significantly nonzero).

Introduction of a sigmoidal nonlinearity $g(u)$ does not change the linear approximation results drastically. Numerical simulations show that noise induces similar synchronous oscillatory activity both in the nonlinear system and in the linearized one [see Fig. 1(b)]. However some classes of nonlinearity can show coherent stochastic resonance phenomena [19]. We categorize the nonlinearity into two general classes (as in Ref. 10) in terms of how g_u deviates from linearity near the fixed point $\overline{\mathbf{u}}$

$$\text{class I: } g_u(u_i) \sim u_i - au_i^3 \quad \text{class II: } g_u(u_i) \sim u_i + au_i^3 - bu_i^5, \tag{11}$$

where $a, b > 0$, and u_i is measured from the fixed point value $\overline{u_i}$. Classes I and II nonlinearity differ in whether the gain g_u' decreases or increases (before saturation) as one moves away from the equilibrium point, and will lead to qualitatively different behavior, as will be shown. Figure 4(b) shows the ratio

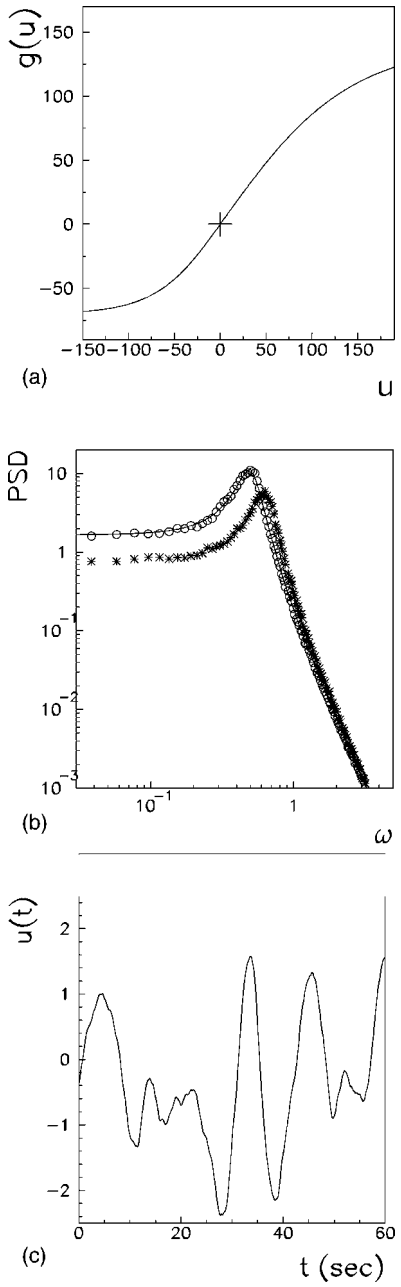

FIG. 1. Numerical simulations of a long-range connectivity [Eq. (3)] model. The values of parameters have been chosen in such a way to satisfy the conditions for the regime B [specifically, $\alpha = 50\ s^{-1}$, $N=10$, $J_{ij}=j_0/N=2(\alpha-0.1)/N$, $W_{ij}=W_0/N$, $H_{ij}=h_0\delta(i-j)$, $W_0=h_0=\sqrt{0.25j_0^2+0.25}$, so that $\omega_0=\sqrt{-j_0^2/4+h_0W_0}=0.5$ rad/s]. (a) Activation function $g(u)$ used in simulations for excitatory units. u is measured from the fixed point value $\overline{u}$, and $g(u)$ is shifted vertically so that the fixed point coincides with the origin (0,0), marked by a cross. (b) Power spectrum density of excitatory units activity, in regime B, with noise $\Gamma=0.0004$. Stars are nonlinear simulations results, circles are linear simulations results, while solid line is theoretical prediction in linear approximation. A broad peak at $\omega\neq 0$ in the PSD is induced by noise. (c) The time behavior of the state variable $u_i(t)$, $i=1,\ldots,N$ in the linear numerical simulation in regime B, with $\Gamma=0.0004$. Lines $u_i(t)$, $i=1,\ldots,N=10$, overlaps each other because of synchrony. All units $u_i(t)$ shows synchronous aperiodic oscillatory activity.

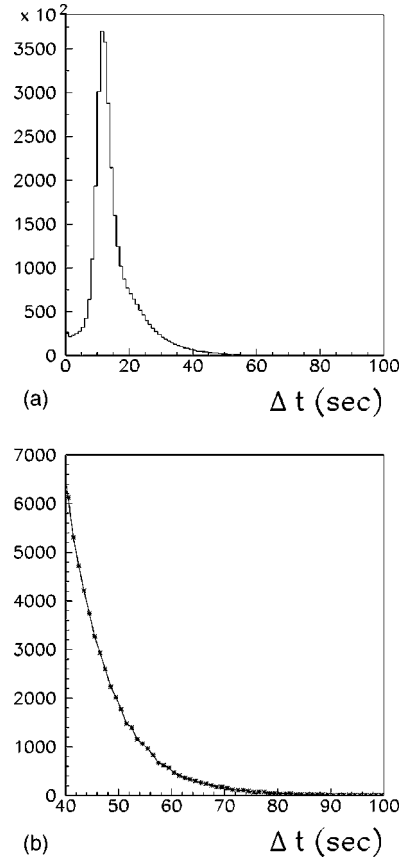

FIG. 2. (a) Histogram of intersynchronous event intervals of the activity shown in previous figure (regime B with $\Gamma=0.0004$). (b) Zoom of the decay region of the IEI histogram.

$R=\tilde{C}(\omega_0)/\Gamma$ between the output power at the characteristic frequency ω_0 and the power of the noise Γ, versus the noise level, using the two nonlinearities shown in Fig. 4(a) (dashed line for class I, solid line for class II), in a long-range connectivity model. Class II nonlinearity can enhance the ratio between the height of the PSD peak and the strength of noise, for a critical range of noise intensities. Solid line in Fig. 4(b) shows the typical maximum that has become the fingerprint of stochastic resonance phenomena [19]. Figure 4(c) shows that the oscillation frequency changes (slowly) with the noise level Γ.

V. REGIME C DYNAMICS

If the excitatory-to-excitatory connections are stronger, so that $\mathrm{Re}[\lambda_{n=0}]=\alpha-j_0/2\geqslant 0$, but not too strong, so that it is still $\mathrm{Im}[\lambda_0]\neq 0$, then spontaneous oscillatory activity arises also without noise. In particular, spontaneous periodic oscillations arise in the linear approximation if $\mathrm{Re}[\lambda_0]=0$ and $\mathrm{Im}[\lambda_0]\neq 0$, this is a critical point separating the regimes $\mathrm{Re}[\lambda_0]<0$, $\mathrm{Im}[\lambda_0]\neq 0$ (regime B) and $\mathrm{Re}[\lambda_0]>0$, $\mathrm{Im}[\lambda_0]\neq 0$ (regime C).

In the regime C linear analysis predicts synchronous periodic activity with diverging amplitude, that becomes stable when nonlinearity is taken into account. We focus on class I nonlinearity [Eq. (11)], when g_u deviates from linearity near

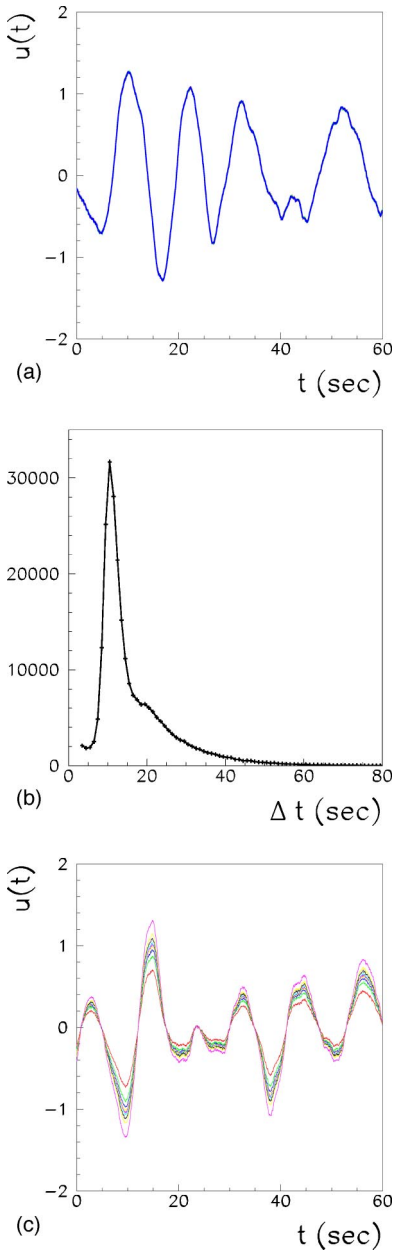

FIG. 3. (Color online) Numerical simulation of a noisy nonlinear square model with structured short-range connectivity in regime B, using periodic boundary condition [Eq. (4)] (a and b) and open boundary conditions (c). $N=100$ excitatory and N inhibitory units are placed on a 10×10 square. The values of parameters have been chosen in such a way to satisfy the conditions for the regime B [specifically, $\alpha=50\ \mathrm{s}^{-1}$, $N=100$, $W_0=h_0=\sqrt{0.25j_0^2+0.25}$, $j_0=2(\alpha-0.1)$, so that $\omega_0=0.5$ rad/s]. (a) The time behavior of excitatory activity $u_i(t)$, $i=1,\ldots,N$ in the model with periodic boundary condition. [Specifically parameters are $J_{ij}=j_0/8$ and $W_{ij}=W_0/8$ for $|i-j|$ mod $N=1,M,M\pm1$, and $H_{ij}=h_0\delta(i-j)$, $\Gamma=0.001$]. (b) Histogram of intersynchronous event intervals of the activity shown in (a). (c) The time behavior of excitatory activity $u_i(t)$, $i=1,\ldots,8$ in the model with open boundary condition. Activity is synchronous, but with different amplitudes. Parameters: $J_{ij}=j_0/7.75$ and $W_{ij}=W_0/7.75$ for $|i-j|=\pm1,\pm M,\pm(M\pm1)$, zero otherwise, $H_{ij}=h_0\delta(i-j)$, $\Gamma=0.04$.

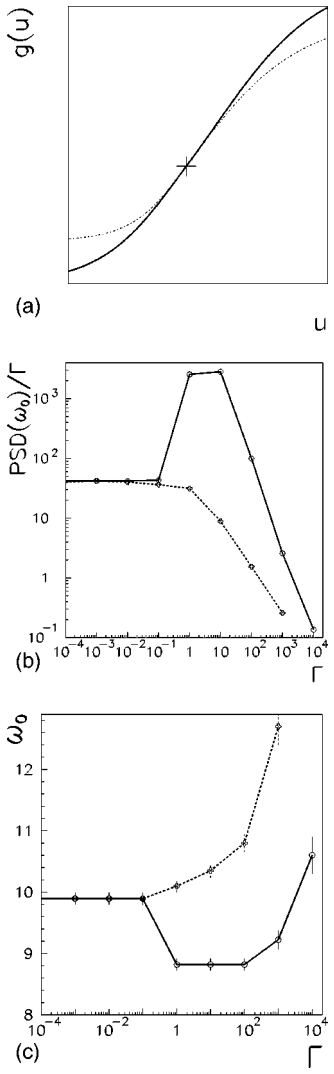

FIG. 4. Nonlinearity and stochastic resonance effects. Numerical simulations of a long-range connectivity model in regime B. (a) Two activation functions for excitatory units u_i. Dashed line shows a saturating activation function (class I, used in most of the following simulations), while solid line shows a class II nonlinear function whose slope increases before decreasing when u is raised from its stationary value (cross). (b) Ratio $R=\mathrm{PSD}(\omega_0)/\Gamma$ as a function of the noise level Γ. Dashed line corresponds to the class I activation function shown with dashed line in (a), while the solid line to the solid line class II activation function. We used the following parameters in the simulations: $N=10$, $\alpha=50\ \mathrm{s}^{-1}$ $J_{ij}=j_0/N=9.98\ \mathrm{s}^{-1}$, $W_0=h_0=50.89\ \mathrm{s}^{-1}$, so that $\omega_0=10$ rad/s. (c) The frequency of the PSD peak versus the noise level [same simulations as in (b)]. Effect of nonlinearity is evident in both (b) and (c), indeed for linear system R and ω_0 do not change with noise level.

the fixed point $\bar{\mathbf{u}}$ due to saturation. This case includes most standard sigmoids used in modeling, including logistic sigmoids, hyperbolic tangent, and rounded threshold-linear models with a soft saturation at high input level. Equation (6) then becomes

$$[(\alpha+\partial_t)^2]\mathbf{u}-[(\partial_t+\alpha)\mathsf{J}-\mathsf{HW}]g_u(\mathbf{u})=-HF(t), \quad (12)$$

where by $g_u(\mathbf{u})$ we mean a vector with components $[g_u(\mathbf{u})]_i=g_u(u_i)$.

Figure 5 shows the simulation results of a long-range connectivity model in regime C, with and without noise. Figure 1(a) shows the saturating function that we have used in our numerical nonlinear simulations for excitatory units. Simulation results of $N=100$ short-range connectivity model with $M=L=10$ in regime C, shown in Fig. 6, are in qualitative agreement with the long-range connectivity model results. As shown in Figs. 5(a) and 6(a) the noiseless nonlinear numerical simulations show stable synchronous periodic oscillatory activity **u**.

We check numerically that this spontaneous periodic oscillations behavior holds only for a particular range of parameters (regime C). For example, starting from the regime C parameters used in Fig. 5, for lower excitatory connections ($j_0=99.86<2\alpha$) we get regime B aperiodic oscillations, while increasing $j0$ beyond the regime C range (e.g., at $j_0=103>\sqrt{h_0 w_0}$) the network jumps to a new stable fixed point (and it starts to oscillate around the new fixed point if there is noise).

As shown in Figs. 5(c) and 6(b) the PSD in regime C has two high peaks at first and second harmonic of the periodic network activity, resembling the experimental results of [5]. Moreover [4] has put in evidence experimentally the existence of a broad peak at low frequencies in the PSD, indicating long time positive correlations. Our model reproduces these results, indeed numerical simulations of regime C in presence of noise, with both type of connectivities, show a broad peak at low frequency in the PSD [see Fig. 5(d)]. The broad peak is absent when the noise is absent. The low frequency's behavior indicates a long-time positive autocorrelation in the activity of the network. This behavior cannot be accounted by the IF model of Segev *et al.* (see Fig. 3(c) in [4]). In order to compare the IEI behavior of our model in the two regimes, the IEI histogram for the noisy model in regime C has been computed (see Fig. 7). It looks totally different from the IEI histogram in regime B. In the regime C, for both the long-range and short-range connectivity cases, the long time tail of the IEI disappears. There is only a narrow high peak corresponding to the period of the signal. Therefore, one prediction of our model is that the experimental IEI at 1 mM Ca concentration should have a high peak (periodicity) with a fast decay similarly to Fig. 5 (differently than at 0.5 mM Ca).

A. Fading of periodicity at long times

Another effect, put in evidence experimentally [5], is the decrease in time of the periodicity of the bursting activity under 1 mM Ca on the time scale of several minutes. According to Segev *et al.* [5], this effect could be related with the possibility of network adaptation, that still needs to be verified experimentally.

In our model we identify two parametric changes which result in a decrease of the periodicity, namely, the increase of noise level and the depression of excitatory connections. The depression of the synapses, during the experiments, could be justified in the light of adaptation processes: shortly after 1 mM Ca is added the excitatory connections increase their

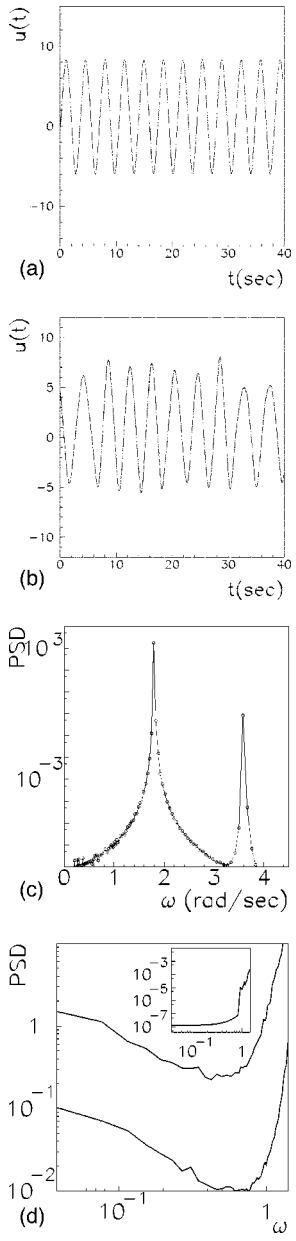

FIG. 5. Regime C simulations of the nonlinear model with long-range connectivity [Eq. (3)]. We use the following parameters $N=10$, $J_{ij}=j_0/N=2(\alpha+0.07)/N$, and $W_0=h_0=\sqrt{0.25j_0^2+0.25}$. The activation function for the excitatory unit is shown in Fig. 1(a). (a),(b) Time behavior of the state variables $u_i(t)$, in the numerical simulation of the isolated EI long-range connectivity network in regime C. [Lines $u_i(t)$, $i=1,..,10$, overlap each other because of synchrony.] (a) Regime C, noiseless nonlinear system. Synchronous periodic oscillatory activity is shown. (b) Regime C, noisy nonlinear system with $\Gamma=0.01$. The activity is almost periodic, but noise decorrelates the signal over long time scales. (c) Power spectrum density of the activity shown in a lin-log scale. The peaks in the first and second harmonic mark clearly the collective periodic activity. (d) Log-log plot of the power spectrum density of the activity in regime C at $\Gamma=0.01$ (upper curve), $\Gamma=0.001$ (lower curve) and $\Gamma=0$ (inset). Noise induces a broad peak at low frequency.

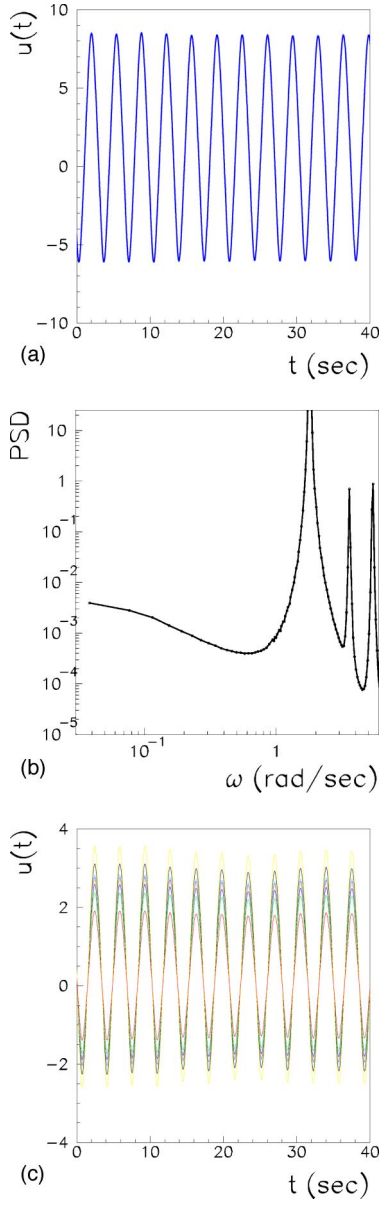

FIG. 6. (Color online) Numerical simulations of nonlinear model with short-range connectivity (4) in regime C, using periodic boundary conditions (a and b) and open boundary condition (c). $N=100$ excitatory and N inhibitory units are placed on a 10×10 square. The values of parameters have been chosen in such a way to satisfy the conditions for regime C (specifically, $N=100$, $j_0=2(\alpha+0.07)$, $W_0=h_0=\sqrt{0.25j_0^2+0.25}$). (a) Time behavior of the state variables $u_i(t)$ (synchrony) in the periodic boundary condition connectivity case (4). [Specifically parameters are $J_{ij}=j_0/8$, $W_{ij}=W_0/8$, for $|i-j|$ mod $N=1,M,M\pm1$, $H_{ij}=h_0\delta(i-j)$.] (b) PSD of the activity $u_i(t)$ shown in (a). (c) Time behavior of the state variable $u_i(t)$ for $i=1,\ldots,10$ in the open boundary condition model. Activities of the units are synchronous but with different amplitudes. [Specifically parameters are $J_{ij}=j_0/7.75$, $W_{ij}=W_0/7.75$, for $|i-j|=\pm1,\pm M,\pm M,\pm1$, $H_{ij}=h_0\delta(i-j)$.]

efficacy, while several minutes after the system possibly adapt to the new concentration and the efficacy of connections decreases to the original values. Also an increase of the noise during time cannot be excluded in principle. Even

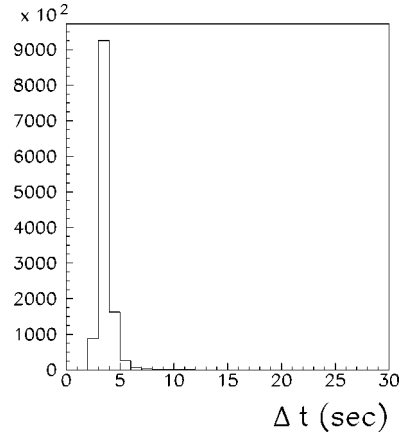

FIG. 7. Histogram of intersynchronous event intervals, of the activity shown in Fig. 5(b) (nonlinear model with long-range connectivity in regime C with $\Gamma=0.01$).

though all conditions, like temperature and humidity, are kept constant during the experiment, an increase of the noise of the system is possible.

So, according to our analysis, adaptation (which is related to the depression of the excitatory connections) is not the only possible explanation of the fading of periodicity observed experimentally, since simply an increase of the level of intrinsic noise is able to account for the observed fading of periodicity.

To show this, we have computed numerically the PSD for different values of the noise and for different values of the excitation. The results are reported in Figs. 8 and 9, respectively. In both figures, it is evident that a fading of periodicity (i.e., a decrease of the first and second harmonic peaks) occurs both when noise increases and when excitatory connections are depressed. Looking at Figs. 8 and 9 we see that the two parametric changes (noise-change or excitatory con-

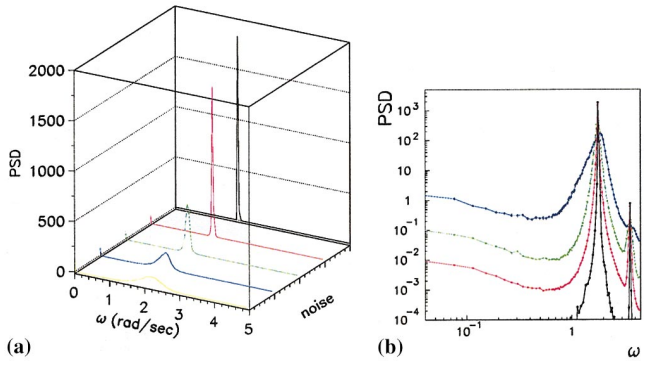

FIG. 8. (Color) (a) Power spectrum density of the excitatory units activity of the noisy nonlinear networks with long-range connectivity in regime C, plotted at different noise levels. Black line: no-noise $\Gamma=0.0$, red line: $\Gamma=0.0001$, green line: $\Gamma=0.001$, blue line: $\Gamma=0.01$, and yellow line: $\Gamma=0.1$. Noise makes the high periodic activity fade away. (b) Log-log plot of the power spectrum densities shown in (a). The two high peaks in the PSD correspond to the first and second harmonics of the activity period. The low frequency power spectrum distribution shows a broad peak in $\omega=0$.

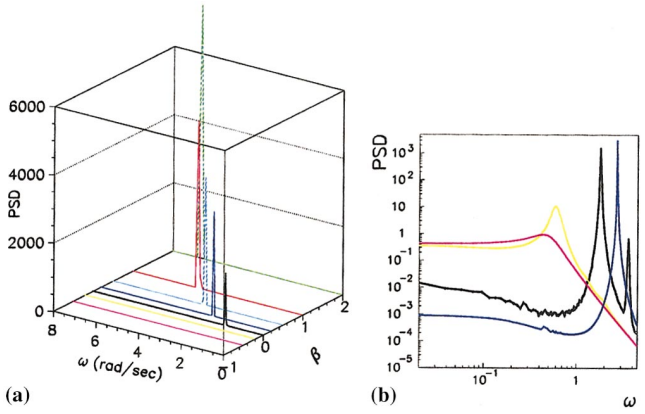

FIG. 9. (Color) (a) Power spectrum density of the excitatory units activity of the noisy nonlinear long-range networks, at $\Gamma=0.0001$, plotted versus β, $j_0=\beta+\overline{j_0}$, $W_0=\beta+\overline{W_0}$ [where $\overline{j_0}=2(\alpha+0.07)$ and $\overline{W_0}=\sqrt{0.25j_0^2+0.25}$ correspond to regime C]. Increasing β the excitatory connections become stronger. Decrease of β (i.e., decrease of excitation) makes the high periodic activity fade away. (b) Log-log plot of some of the power spectrum densities shown in (a). Blue line: $\beta=0.2$ back line: $\beta=0$; yellow line: $\beta=-0,2$; and magenta line: $\beta=-0.5$. The two high peaks in the PSD correspond to the first and second harmonics of the activity period. The low frequency power spectrum distribution shows a broad peak in $\omega=0$ that decreases when excitation (β) decreases, fading away.

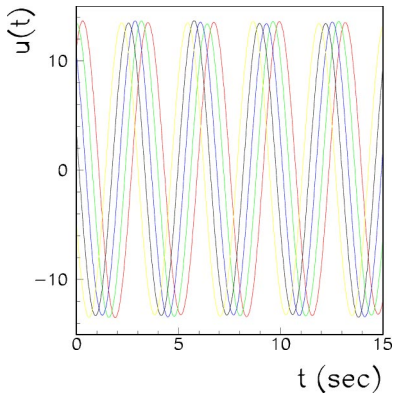

FIG. 10. (Color online) Phase-lock oscillatory activity $u_i(t)$, $i=1,\ldots,5$. $N=100$ excitatory and N inhibitory units are placed on a 10×10 square. J_{ij} and W_{ij} are positive when $|i-j|$ mod $N=1,M,M\pm1$ and are negative when $|i-j|$ mod $N=3,3M,3M\pm1$, all the other elements are null. $H_{ij}=h_0\delta_{ij}$ as usual. The values of parameters have been chosen in such a way to satisfy the conditions for the regime C.

nections decrease) can be discriminated since their effects on the PSD are different at low frequency. In Fig. 8 we note that an increase of the level of noise leads to an increase of the broad peak at $\omega=0$. Instead in Fig. 9 it is evident that a depression of the excitatory connections eigenvalues j_0, W_0 induces a decrease of both the high peaks and the broad peak at $\omega=0$.

However, the experimental results at present do not allow us to discriminate between the two possible explanations because, as far as we know, there is not any measurement of the low frequency PSD after the fading of periodicity occurring on the time scale of several minutes. It could also be that both the phenomena occur and contribute to the fading of periodicity.

An indication that noise may change during time comes from the work of Tateno *et al.* [7] showing the PSD of the activity of a rat cortical network after 12, 18, and 58 days in-vitro (DIV). While PSD at 12 DIV seems to correspond to a noiseless or low-noise system, the figures at 18 and 58 DIV bring to mind the possibility that the noise is increased (in particular a low frequency peak becomes visible, even though the lin-log scale does not highlight it). A strong decrease of periodic activity occurs as number of days increases.

B. Phase-locking between excitatory and inhibitory population

Besides the periodic synchronous bursting activity analyzed until now, our model can exhibit periodic but not synchronous bursting activity. This appears when there is a phase lock between neurons involved in the burst. Mathematically it is described by $u_i(t)\propto|\xi_i|\cos(\omega_0 t-\phi_i)$. We can describe both synchronous and phase-locked periodic activities cases by writing $u_i(t)=\xi_i e^{-i\omega_0 t}+\text{c.c.}$, taking the ξ_i real in the first case and complex ($\xi_i=|\xi_i|e^{i\phi_i}$) in the second.

A phase locked oscillation arises when the dominant eigenvector is complex. Figure 10 shows spontaneous oscillatory activity in regime C with a phase shift $\phi_i=20\pi/Ni$, between all the units u_i involved in the oscillation. This is achieved using both positive and negative connections. Negative connections can be simply implemented via inhibitory interneurons with very short time membrane time constants.

In all simulations of previous sections the excitatory activity is synchronous, while the excitatory population and inhibitory population periodic activity are phase locked, and the phase shift between the two ensembles depends from network parameters. In all the simulations of the previous figures the $u(t)$ versus $v(t)$ phase shift is about few thousandths of a period, in good agreement with the theoretical result $arctg(\omega_0/\alpha)$ coming from the linear approximation analysis of our model. In the experiments of Segev *et al.* [4,5] all the oscillatory population (both excitatory and inhibitory) appear synchronous. Indeed the predicted phase-shift is so tiny that they cannot be clearly distinguished from zero.

VI. SUMMARY AND CONCLUSIONS

In the present paper we analyzed the effect of uncorrelated white noise on the spontaneous dynamics of the EI model. First, we studied the evolution of the system in the linear approximation and put in evidence the existence of two different regimes, B and C. The transition from the B to C regimes is induced by increasing the strength of the excitatory synapses. Then nonlinear corrections have been introduced numerically. The noise induces in the two regimes very different behaviors. In regime B the presence of noise induces collective synchronous aperiodic oscillations in the

neural activity. In this regime nonlinearity does not change the synchronous oscillatory activity but can induce stochastic resonance.

In regime C stable spontaneous periodic oscillations can arise only in the presence of nonlinearity. The oscillations are present also in noiseless conditions. The noise produces a broad peak at low frequency and a fading of periodicity at high level of noise.

The stochastic model presented is able to account for the experimental results of Segev *et al.* In particular it accounts for both the observed synchronous periodic regime (at 1.0 mM Ca concentration—regime C) and aperiodic regime (at 0.5 and 2.0 mM Ca concentration—regime B), and transition from one regime to another. It accounts for the long time positive correlations of the bursting activity, the IEI and spectral features of the activity, and the observed fading of periodicity.

All to all connection matrices whose elements are rescaled with N is a very simplified model that, even though useful for analytical calculations, is not realistic. Recent estimation of connectivity in in-vitro rat cortical networks has shown arborization of the neurons of 1.2 ± 0.5 mm^2 [7]. A more plausible connection matrix for our model therefore is a structured finite range connection structure. We have simulated a network of 100 excitatory and 100 inhibitory units: each couple of excitatory and inhibitory units is placed in a square lattice. Apart from the units on the boundary, each excitatory unit is connected to its four nearest neighbors and to its four next-nearest neighbors. Inhibitory-to-excitatory connections H are still local, with each inhibitory unit connected to only one excitatory unit.

In this structured short-range connections framework we can also account for the size-independence of the activity networks. Indeed Segev *et al.* [4] observe a similarity in the activity of different-size networks. In order to account for this invariance, they suggested that the networks have a self-regulation process that can be achieved, for example, by an adjustment of neural efficacies or neuronal firing threshold. However, the similarity of activity finds a simple explanation in the scenario where each unit is connected only to other units that are within a critical radius. While in an all-to-all connection model, in order to keep the activity constant the strength of the connections should scale with the size of the model, in a short-range connection model the strength of connections should not scale with the network's size. In order to scale the strength of connections with the size of the network a sort of self-regulations should be invoked. In the short-range model we get the scale-invariant activity as a bonus. Indeed the strength of the principal eigenvalue depends on the number of connections for each unit in average, and not on the total number of units.

According to our model, networks with one size too small with respect to the range of connections (such that boundary effects become relevant and affect the average number of connections for each unit) shows dissimilarity from the larger networks activity, at the same environment conditions (same Ca concentration, density, etc).

Finally it is worth mentioning two points.

(i) The occurrence of different regimes of activity in in-vitro cortical networks has been also shown in the recent work of Tateno *et al.* [7]. Figure 6(a) of Ref. [7] shows the PSD that we recognize as typical of regime C, while, for example, we recognize indications of a possible broad peak at low frequency in the PSD shown in Figs. 7(b) and 7(c).

(ii) The "anomalous" low frequency broad peak in the PSD of neural activity is not specific to cortical in-vitro networks, it has been observed in-vivo, for example, in the pulse trains of nerve cells belonging to various brain structures (such as auditory nerve [20] and the mesencephalic reticular formation [21]) and in IF models [22]. In [22] it has been related to the metastability of high activity patterns in the presence of noise (patterns that diffuse throughout the system). The "anomalous" peak has been also pointed out recently in the activity of the suprachiasmatic nucleus [23]. It corresponds to an "anomalous" behavior of the Fano factor at large times. We claim that in the suprachiasmatic nucleus neurons, as in the rat cortical cultures, the low frequency peak in the PSD is just the result of the interplay between nonlinearity and the intrinsic noise.

ACKNOWLEDGMENT

We would like to thank Ronen Segev for useful discussions.

[1] H. Kamioka, E. Maeda, E. Jimbo, H.P.C. Robinson, and A. Kawana, Neurosci. Lett. **206**, 109 (1996).

[2] A. K. Engel, P. Konig, A. K. Kreiter, T. B. Schillen, and W. Singer, Trends Neurosci. **15**, 218 (1992).

[3] M. Canepari, M. Bove, E. Maeda, M. Cappello, and A. Kawana, Biol. Cybern. **77**, 153 (1997).

[4] R. Segev, M. Benveniste, E. Hulata, N. Cihen, A. Palevski, E. Kapon, Y. Shapira, and E. Ben-Jacob, Phys. Rev. Lett. **88**, 118102 (2002).

[5] R. Segev, Y. Shapira, M. Benveniste, and E. Ben-Jacob, Phys. Rev. E **64**, 011920 (2001).

[6] G. W. Gross, and F. U. Schwalm, J. Neurosci. Methods **52**, 73 (1994).

[7] T. Tateno, A. Kawana, and Y. Jimbo, Phys. Rev. E **65**, 051924 (2002).

[8] M. S. Jensen and Y. Yaari, J. Neurophysiol. **77** 1224 (1997); Ann. Neurol. **24**, 591 (1988).

[9] H. R. Wilson and J. D. Cowan, Kybernetik **13**, 55 (1973); Biophys. J. **12**, 1 (1972).

[10] S. Scarpetta, L. Zhaoping, and J. Hertz, Neural Comput. **14**, 2371 (2002); S. Scarpetta, L. Zhaoping, and J. Hertz, in *NIPS 2000*, Vol. 13, edited by T. Leen, T. Dietterich, and V. Tresp (MIT, Cambridge, MA, 2001).

[11] Y. Shim, H. Hong, and M. Y. Choi, Phys. Rev. E **65**, 036114 (2002).

[12] W. Gerstner, Neural Comput. **12**, 43 (2000).

[13] A. S. Pikovsky and J. Kurths, Phys. Rev. Lett. **78**, 775 (1997).
[14] P. Dayan and L. F. Abbott, *Theoretical Neuroscience* (MIT Press, Cambridge, 2001).
[15] R. Segev, M. Benveniste, Y. Shapira, and E. Ben-Jacob, Phys. Rev. Lett. **90**, 168101 (2003).
[16] J. Opher and D. Horn, Neurocomputing **32**, 161 (2000).
[17] C. Koch, *Biophysics of Computation* (Oxford University Press, New York, 1999).
[18] I. B. Levitan and L. K. Kaczmarek, *The Neuron* (Oxford University Press, New York, 1991).
[19] C. Zhou, J. Kurths, and B. Hu, Phys. Rev. Lett. **87**, 98101 (2001);L. Gammaitoni, P. Hanggi, P. Jung, and F. Marchesoni, Rev. Mod. Phys. **70**, 223 (2001).
[20] M. C. Teich, IEEE Trans. Biomed. Eng. **36**, 150 (1989).
[21] F. Grueneis, M. Nakao, and M. Yamamoto, Biol. Cybern. **62**, 407 (1990).
[22] M. Usher, M. Stemmler, and Z. Olami, Phys. Rev. Lett. **74**, 326 (1995).
[23] S. Kim, J. Jeong, Y. Kwak, and K. Lee, in *Computational Neuroscience CNS*2002*, edited by E. De Schutter (Elsevier, New York, 2002).